Supporting Information:
Information Dense And Industry Scalable Accelerated Formation

Leon Merker [1,2,3,4], *Markus Blessing [5], Bojing Zhang [3,4], Helge Sören Stein [3,4]*

1: Helmholtz Institute Ulm, Helmholtzstr. 11, 89081 Ulm, Germany
2: Karlsruhe Institute of Technology, 76021 Karlsruhe, Germany
3: Technical University of Munich, Germany, Lichtenbergstr. 4, 85748 Garching; TUM School of Natural Sciences, Department of Chemistry, Chair of Digital Catalysis; Munich Institute of Robotics and Machine Intelligence (MIRMI); Munich Data Science Institute (MDSI), Munich Institute of Integrated Materials, Energy and Process Engineering (MEP)
4: Munich Center for Machine Learning (MCML), Oettingenstraße 67, 80538 München, Germany
5: Zentrum für Sonnenenergie- und Wasserstoff-Forschung Baden-Württemberg Ulm, Ulm, Germany

*Correspondence should be addressed to: leon.merker@tum.de, helge.stein@tum.de

Test protocol and formation

All cells ran through the same test protocol which is exemplary shown for pulsed formation in figure S1. After 24h wetting time, the formation was started using either constant current or the pulses depicted in figure S2.
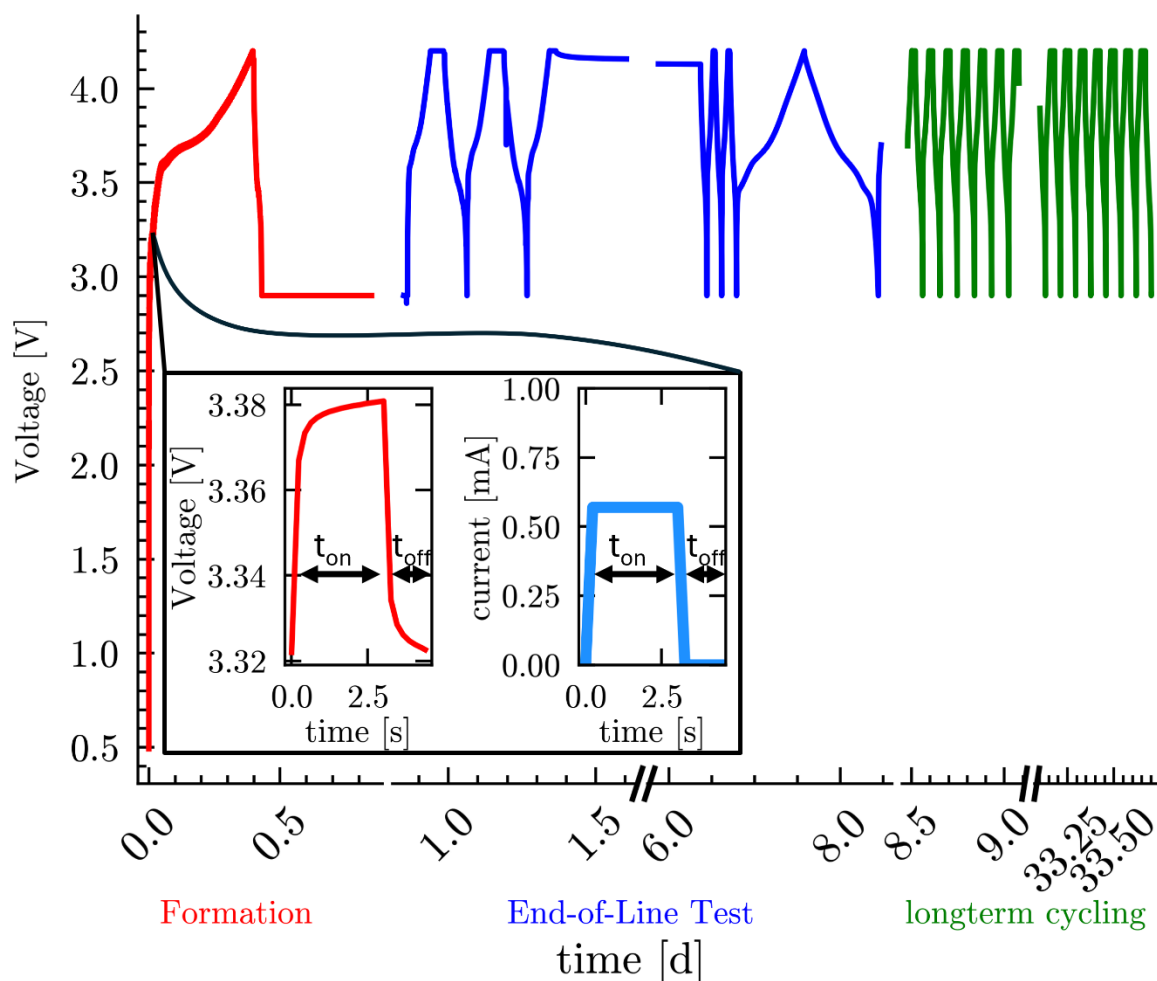

Figure S1. presents the voltage curve including the formation, the End-of-Line test and exemplary cycles for a nickel manganese cobalt (NMC) (622) | graphite coin cell using C/5.7 current pulses (t_{on} = 3 s, t_{off} = 1.33 s, and current i = C/5.7). An exemplary pulse and voltage response within the formation is plotted in the small window.
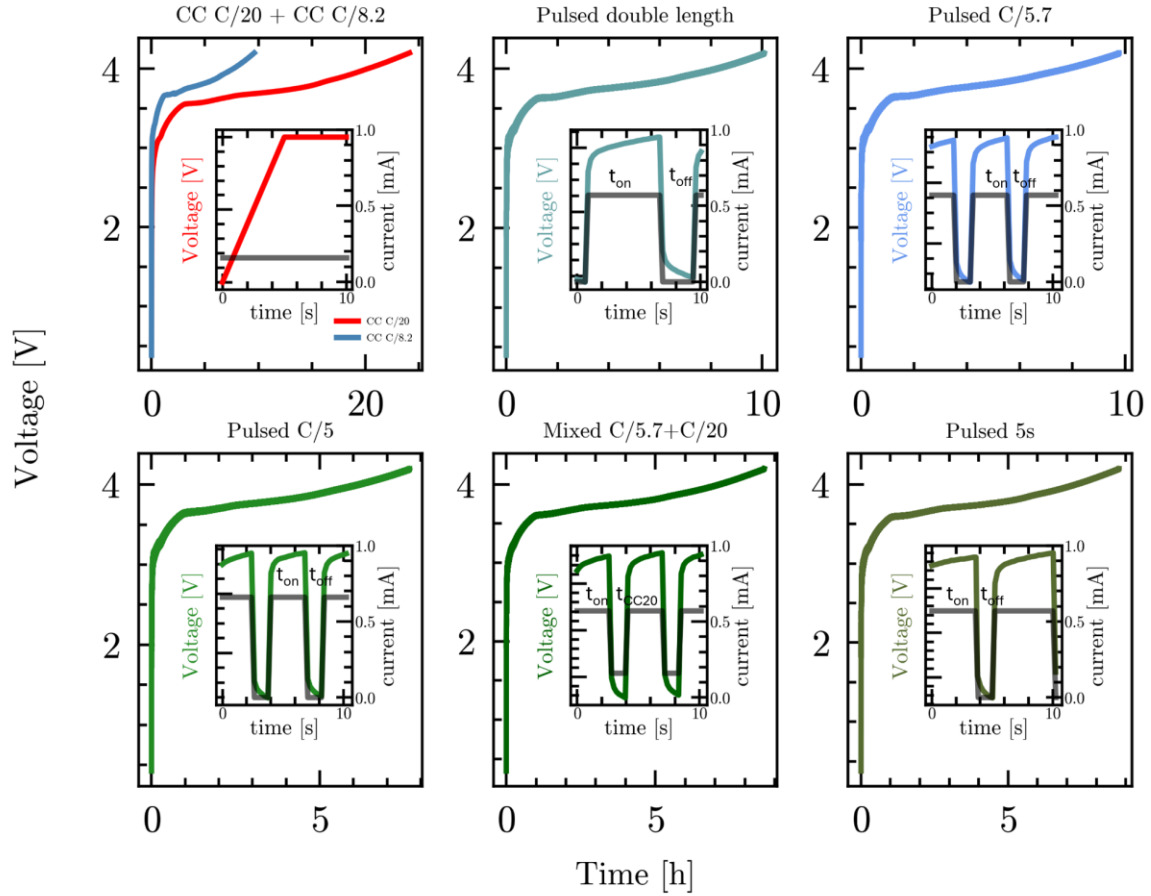
Figure S2. *presents exemplary charging curves associated with the formation of the solid electrolyte interphase (SEI) in a nickel manganese cobalt (NMC) (622) | graphite coin cell. The red curve, which represents a common constant current (CC) charging method at a rate of C/20, serves as reference. The first subset of accelerated formation times is illustrated by the blue plots, which exhibit an effective C-rate of 8.2. Within this subset, CC charging at C/8.2 has been selected for direct comparison. Conversely, the cells employ a pulsed charging approach at C/5.7 (with a duration of t_{on} = 3 s, t_{off} = 1.33 s, and current i = C/5.7). Furthermore, the analysis includes a pulsed strategy characterized by double the duration (t_{on} = 6 s, t_{off} = 2.66 s, i = C/5.7) to evaluate its effective C-rate and explore the potential influence of the ton/off ratio. The second subset, characterized by the greenish plots, corresponds to even shorter formation times and achieves effective C-rates of approximately C/7.2. In this subset, the formation current is increased using a pulsed C/5 (t_{on} = 3 s, t_{off} = 1.33 s, i = C/5), alongside a mixed strategy that combines C/5.7 and C/20 (t_{on} = 3 s, i_{on} = C/5.7, t_{CC20} = 1.33 s, i_{CC20} = C/20) as well as an increased ton pulsed duration of 5 s (t_{on} = 5 s, t_{off} = 1.33 s, i = C/5.7). Detailed analysis, including zoomed-in plots of voltage and current profiles, clarifies the distinctions among these charging strategies.*

End-of-Line test

For all box-plots, the green horizontal line within the boxes indicates the median. The box represents the range of the middle 50% of the data. The whiskers reveal the minimum and maximum up to 1.5 times of the box range. Circles outside the whiskers are considered as outliers, as they lie outside of the 75% percentile range. The following plots S3, S4 and S5 present the determined capacity of the capacity checks of the EOL using 1C CCCV charging which C/20 current cutoff value and 1C discharging. Note, that the second and third capacity check were performed after the Hybrid Pulse Power Characterization (HPPC) test to determine the internal resistance and the self-discharge test.
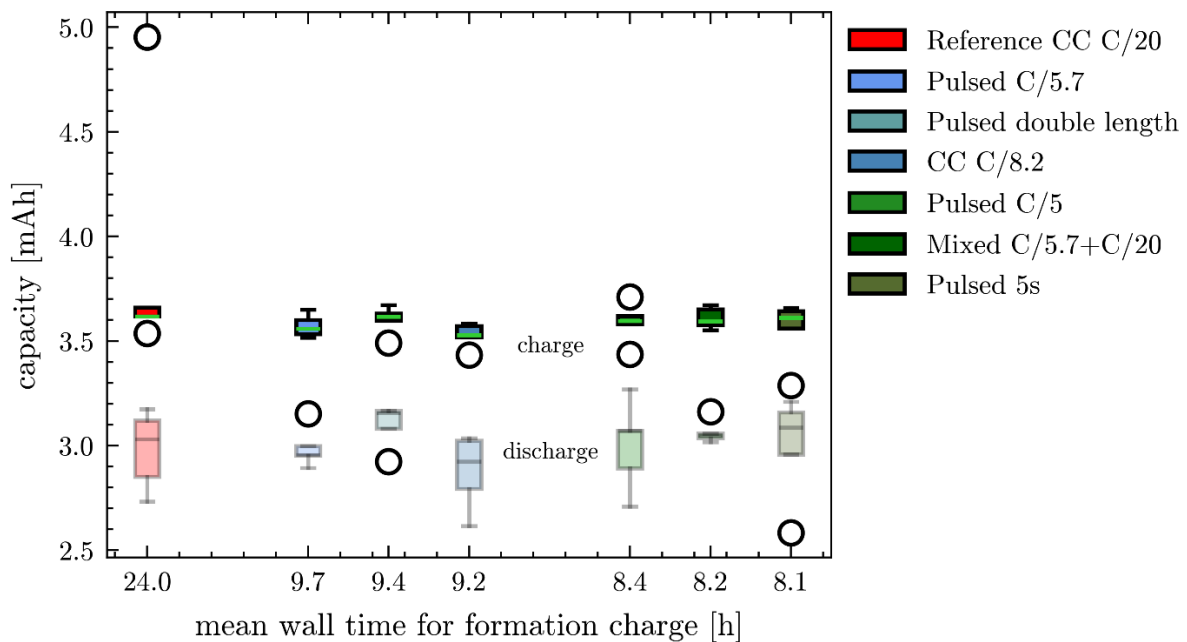

Figure S3. Box plots of the measured absolute charge(colored) and discharge(transparent) capacities of the first capacity check following the formation with C/2 charge and discharge rate. 5 cells of each formation strategy were considered, and boxes are sorted by their mean wall time of the formation charge. All mean charge capacities are within the same small range, whereas discharge capacities differ more in mean values and box size.
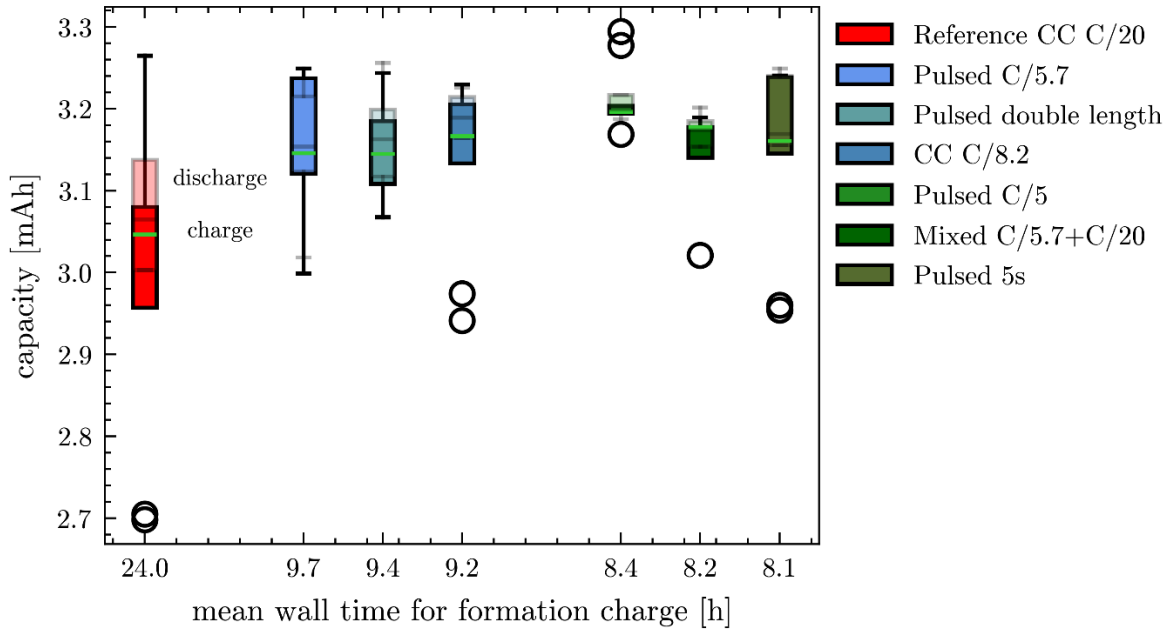
Figure S4. Box plots of the measured absolute charge(colored) and discharge(transparent) capacities of the second capacity check following the self-discharge measurement of the EOL test with C/2 charge and discharge rate. 5 cells of each formation strategy were considered, and boxes are sorted by their mean wall time of the formation charge. Charge and discharge values strongly overlap for the individual strategies and median values are within the same range except for reference CC C/20 cells with conspicuously low values. Median discharge capacities are higher for all strategies as an effect of the anode overhang[1][2][3][4][5].
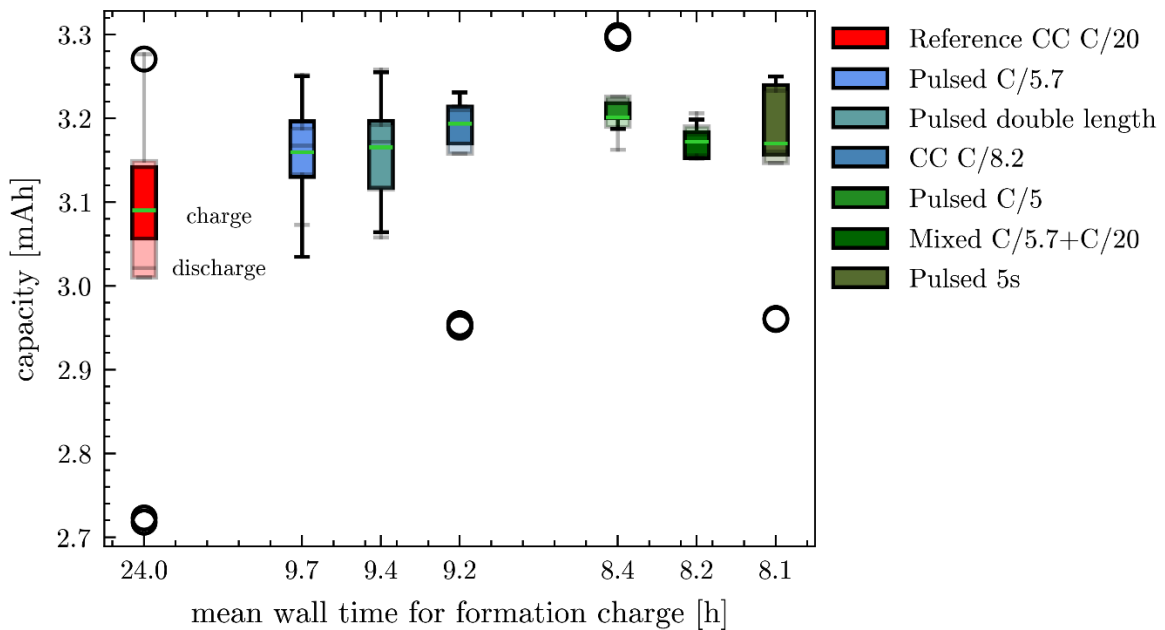

Figure S5. Box plots of the measured absolute charge(colored) and discharge(transparent) capacities of the third capacity check following the second capacity check with C/2 charge and discharge rate. 5 cells of each

formation strategy were considered, and boxes are sorted by their mean wall time of the formation charge. Charge and discharge values strongly overlap for the individual strategies and median values are within the same range except for reference CC C/20 cells with lower values. Median discharge capacities are still higher for some strategies as an effect of the anode overhang[1][2][3][4][5].
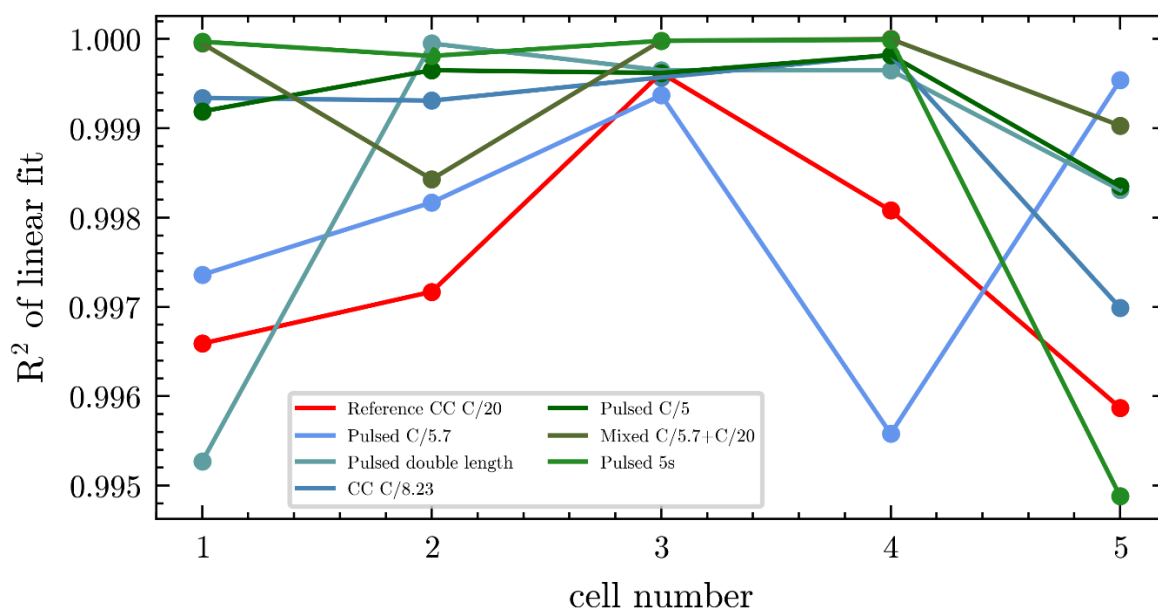

Figure S6. R^2-values of the linear fits of the self-discharge voltage after 24h relaxation versus the square root of time over the cell number.
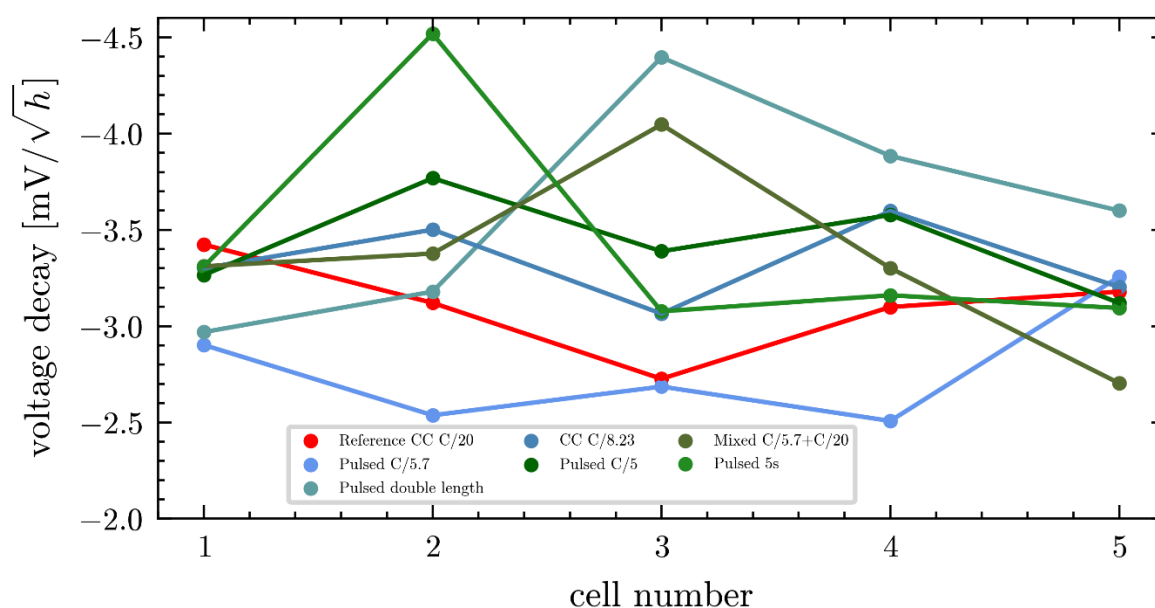

Figure S7. Voltage decay values determined as the slope of the linear fits of self-discharge voltage after 24h relaxation versus the square root of time for all formation strategies.
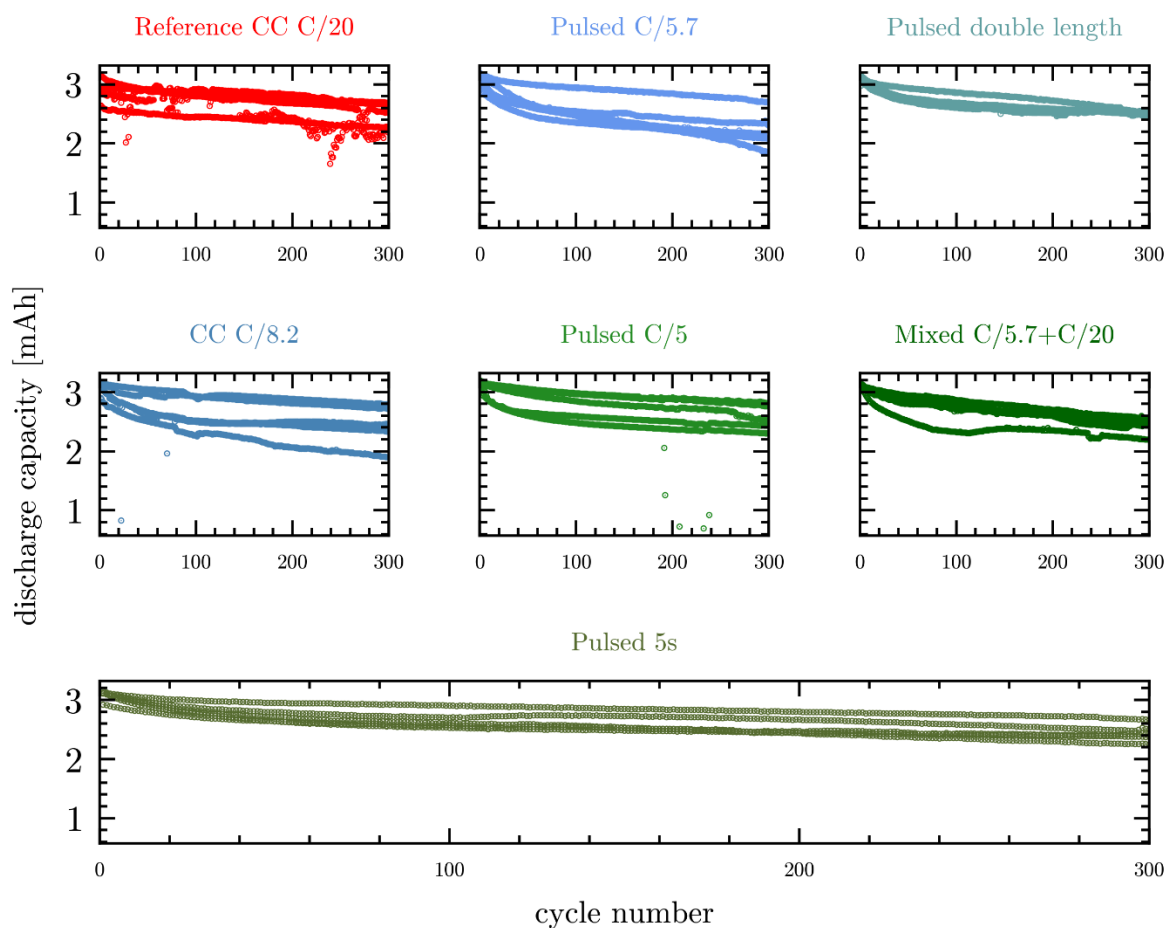
Longterm cycling

Figure S8. Discharge capacities over 300 cycles of 5 cells of each formation strategy after formation and EOL test. Cycles were performed using 1C for charge and discharge. All strategies show a larger drop of capacity in the first cycles followed by more linear decrease. Large scattering of remaining capacity can be observed for the reference CC C/20 cells but also for most pulsed formed cells. All cells show starting capacities around 3.2 mAh, which is in good agreement the theoretical calculated capacity of 3.27 mAh.
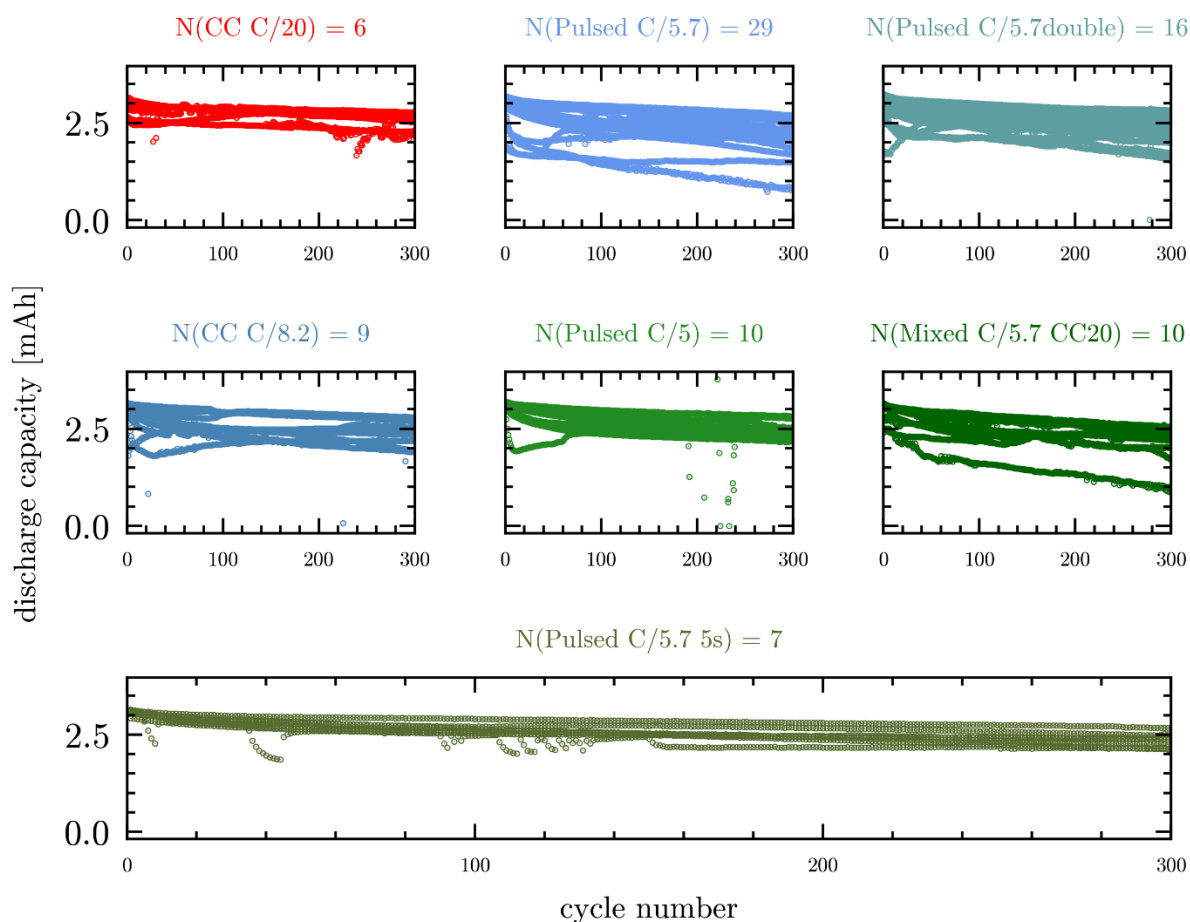
Figure S9. Discharge capacities over 300 cycles of all cells tested of each formation strategy after formation and EOL test. Cells were cycled using 1C current for charge and discharge. Number of cells are indicated above the respective plot. All strategies show a larger drop of capacity in the first cycles followed by more linear decrease. All strategies show large variance in starting and remaining capacity after 300 cycles.

Conflicts of Interest

Among others, LM, BZ, and HSS are named inventors on a related patent application published under WO2024170596 with the title "METHOD AND DEVICE

FOR FORMING AN ELECTROCHEMICAL DEVICE" and may benefit through Arbeitnehmererfindergesetz ArbnErfG, specifically §40. Patenting rights are owned by Karlsruher Institut für Technologie.

References

[1]   Hüfner, T., Oldenburger, M., Beduerftig, B., & Gruhle, A. (2019). Lithium flow between active area and overhang of graphite anodes as a function of temperature and overhang geometry. *Journal of Energy Storage*, *24*, 100790.

[2]   Lewerenz, M., Fuchs, G., Becker, L., & Sauer, D. U. (2018). Irreversible calendar aging and quantification of the reversible capacity loss caused by anode overhang. *Journal of Energy Storage*, *18*, 149-159.

[3]   Lewerenz, M., Münnix, J., Schmalstieg, J., Käbitz, S., Knips, M., & Sauer, D. U. (2017). Systematic aging of commercial LiFePO4| Graphite cylindrical cells including a theory explaining rise of capacity during aging. *Journal of power sources*, *345*, 254-263.

[4]   Gyenes, B., Stevens, D. A., Chevrier, V. L., & Dahn, J. R. (2014). Understanding anomalous behavior in coulombic efficiency measurements on Li-ion batteries. *Journal of The Electrochemical Society*, *162*(3), A278.

[5]   Smith, A. J., Burns, J. C., Trussler, S., & Dahn, J. R. (2009). Precision measurements of the coulombic efficiency of lithium-ion batteries and of electrode materials for lithium-ion batteries. *Journal of The Electrochemical Society*, *157*(2), A196.